Heating rates in collisionally opaque alkali-metal atom traps: Role of secondary collisions

H. C. W. Beijerinck

Physics Department, Eindhoven University of Technology, P.O. Box 513, 5600 MB Eindhoven, The Netherlands

Grazing collisions with background gas are the major cause of trap loss and trap heating in atom traps. To first order, these effects do not depend on the trap density. In collisionally opaque trapped atom clouds, however, scattered atoms with an energy E larger than the effective trap depth $\mathcal{E}_{\mathrm{eff}}$, which are destined to escape from the atom cloud, will have a finite probability for a secondary collision. This results in a contribution to the heating rate that depends on the column density $\langle nl \rangle$ of the trapped atoms, i.e., the product of density and characteristic size of the trap. For alkali-metal atom traps, secondary collisions are quite important due to the strong long-range interaction with like atoms. We derive a simple analytical expression for the secondary heating rate, showing a dependency proportional to $\langle nl \rangle \; \mathcal{E}_{\mathrm{eff}}^{1/2}$. When extrapolating to a vanishing column density, only primary collisions with the background gas will contribute to the heating rate. This contribution is rather small, due to the weak long-range interaction of the usual background gas species in an ultrahigh-vacuum system—He, Ne, or Ar—with the trapped alkali-metal atoms. We conclude that the transition between trap-loss collisions and heating collisions is determined by a cutoff energy $200 \; \mu\mathrm{K} \lesssim \mathcal{E}_{\mathrm{eff}} \lesssim 400 \; \mu\mathrm{K}$, much smaller than the actual trap depth $\mathcal{E}$ in most magnetic traps. Atoms with an energy $\mathcal{E}_{\mathrm{eff}} < E < \mathcal{E}$ escape into the Oort cloud: a mechanism of effective traploss in the microkelvin range of trap temperatures. We present results of secondary heating rates for the alkali-metal atoms Li through Cs as a function of the effective trap depth, the column density of the trap, and the species in the background gas. The predictions of our model are in good agreement with the experimental data of Myatt for heating rates in high-density [87]Rb-atom magnetic traps at JILA, including the effect of the rf shield and the composition of the background gas. It is shown that collisions with atoms from the Oort cloud also contribute to the heating rate. For [85]Rb the calculated heating rate is below the experimentally observed value at JILA, supporting the idea that inelastic collisions in the trap are the major source of heating.

I. INTRODUCTION

The road to Bose-Einstein condensation (BEC) in a dilute sample of trapped alkali-metal atoms is well known: cold atoms are first trapped in a magneto-optical trap, and then transferred to a magnetic trap where evaporative cooling is applied to achieve the ultralow temperatures in the 1 μK to 10 nK range, where the transition to BEC takes place [1–3]. For magnetic trap densities in the range $n \lesssim 10^{14}$ cm^{-3}, collisions with the background gas at ambient temperature are the dominant mechanism of trap loss: the energy transferred in these collisions is much larger than the trap depth. However, for collisions with a scattering angle of a few mrad, the energy transfer is of the same order of magnitude as the trap depth. These atoms do not leave the trap, but dissipate their energy in thermalizing collisions with other trapped atoms. All models predict a heating rate that does not depend on either the trap density or the trap size: only the trap depth plays a role, together with the density and composition of the background gas. In a recent paper we calculated the heating rate for like-particle collisions in low-density traps [4], resulting in a good agreement with experimental data on Cs in a far-off-resonance-trap [5].

The heating rate in magnetic traps of alkali-metal atoms, as used for achieving BEC, shows a very different picture. Most data are available for Rb, the workhorse in this field. In most cases, the experimentally observed heating rate depends on either the density in the trap or the column density, i.e., the product of trap density and trap dimensions. Extrapolating to zero density, the heating rate is rather small or it

even vanishes. These observations are in strong disagreement with the available models for trap heating, which all predict a heating rate that does not depend on trap density or trap size [4,6].

The goal of this paper is to provide a model for trap heating that can explain experimental observations in magnetic traps. The excellent overview of heating mechanisms, as given by Myatt [7] and Cornell *et al.* [8], has served as a source of inspiration. At low densities, the background gas will consist of mostly He, Ne, and Ar, the usual constituents of an ultrahigh-vacuum system that is pumped by an ion-getter pump and a titanium sublimation pump. These background-gas–alkali-metal systems have a small value of the long range van der Waals coefficient C_6 as compared to the like alkali-metal–alkali-metal systems. The small value of C_6 results in a small-angle differential cross section with a large diffractive regime [4,6,9,10], with the net result that only a small fraction of the total cross section results in collisions with an energy transfer less than the trap depth, i.e., trap heating [4,6].

With increasing column density of the trap, a new process of heating will start to be effective. We now enter the regime of a collisionally opaque trap. Primary collisions with an energy transfer to an alkali-metal atom that is *larger* than the trap depth will also start to contribute to the heating process. The low-energy alkali-metal atom produced in these primary collisions, with an energy in the range of 10 mK to 10 K or more, has a finite chance for a secondary collision with a trapped alkali-metal atom before leaving the trap. This re-
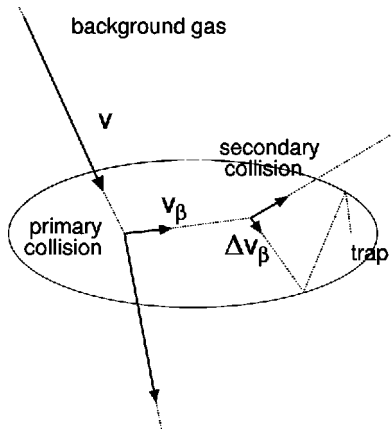
FIG. 1. The background-gas atom with velocity v transfers a velocity v_β to a trapped alkali-metal atom, resulting in a kinetic energy larger than the trap depth; before leaving the trap, this atom can collide with another trapped alkali-metal atom, resulting in a transfer of velocity Δv_β with a corresponding kinetic energy less than the trap depth, thus remaining trapped and contributing to a heating of the trap population by a series of successive thermalizing collisions inside the trap.

sults in an extra transfer of energy to the trapped population, proportional to the column density of the trap. This contribution will thus dominate the heating rate for large values of the column density.

The driving force for any heating of the trap population is the primary collision rate $\dot{\mathcal{N}}$. This holds for heating by primary collisions as well as for heating by secondary collisions. The general physical picture of primary and secondary collisions is given in Fig. 1. In a primary collision, the particle from the background gas with energy E_b and velocity v collides with a cold alkali-metal atom inside the trap. This results in a transferred velocity in the laboratory system equal to v_β with a kinetic energy $E_\beta = \frac{1}{2} m v_\beta^2$. The background-gas atom will then leave the trap without any further collision.

When E_β is less than the trap depth $\mathcal{E}$, the target atom will not leave the trap and thermalize to the equilibrium temperature of the trap. As a result, these primary collisions will contribute to heating of the trap population. When E_β is larger than the trap depth $\mathcal{E}$, the scattered alkali-metal atom still has a finite chance to collide with another trapped alkali-metal atom, resulting in a secondary collision with another trapped atom. In the laboratory system, the transferred velocity is equal to Δv_β with a kinetic energy $\Delta E_\beta = \frac{1}{2} m (\Delta v_\beta)^2$. For energies ΔE_β less than the trap depth $\mathcal{E}$, these secondary collisions will also lead to a heating of the trap population. Assuming small-angle scattering in the center-of-mass system, the velocity Δv_β in the laboratory system is then oriented in a direction roughly parallel or antiparallel to the initial velocity v of the background atom, which is the cause of all this happening.

The transfer of energy in a secondary collisions in the 10 mK to 10 K range is very efficient: first, the small-angle differential cross section at these low energies is very large; second, it concerns like-atom collisions of alkali-metal atoms

with a very strong long-range interaction. For example, for Rb atoms with an energy of 1 K, the total cross section is equal to 7.4×10^3 Å^2. At a density of 2×10^{14} cm^{-3}, which is easily obtained experimentally in a trap close to the transition to BEC, the mean free path for secondary collisions then is equal to 68 μm. Comparing this result with a characteristic trap size of 10–30 μm, it is clear that secondary collisions cannot be neglected for a thorough understanding of heating rates.

In this paper we investigate the energy-transfer rate by secondary collisions in the collisionally opaque trap regime. The results for the energy-transfer rate by secondary collisions are given as simple analytical formulas which can be directly applied to a specific trap geometry, using the composition of the background gas and the measured trap-loss lifetime as input. Typical results are given for traps of the alkali-metal gases Li through Cs, with He, Ne, and Ar, and the corresponding alkali-metal atom as most likely constituents of the background gas.

This paper is organized as follows. In Sec. II we derive the formulas for the energy-transfer rate in secondary collisions, based on the energy-transfer integral as derived in a previous paper [4]. In Sec. III we investigate the scaling of the energy-transfer integral of the secondary collisions with the kinetic energy of the projectile, to arrive at an approximate analytical expression for the energy-transfer rate by secondary collisions. In Sec. IV we discuss the analytical expression for the energy-transfer rate, showing the scaling on the properties of the trap atoms, the background gas, the column density, and the trap-loss lifetime. Then, in Sec. V, we refine our definition of heating collisions, with emphasis on the poor coupling of trapped atoms with an energy slightly less than the trap depth to the cold trapped atoms with an energy much less than the trap depth. This is usually referred to as the ''Oort cloud'' paradigm. Before we compare our model calculations with experimental results, we present the appropriate expressions for relating the density, temperature and trap parameters to the correct value of the column density (Sec. VI). In Sec. VII we compare our calculated values to the available data for heating in ^{87}Rb magnetic traps at JILA.[1] In Sec. VIII we investigate the collisional coupling of the atoms in the Oort cloud with the sample in the center of the trap. In Sec. IX we compare the experimental results for the heating rates in ^{85}Rb traps with our calculated values. Finally, concluding remarks are given in Sec. X.

II. SECONDARY COLLISIONS

In this section we investigate the basic ingredients for an analytical description of the heating rate by secondary collisions. First we derive a suitable expression for the total energy input $\dot{U}$ to the trapped sample of cold gas. Next, we investigate the parameters that enter this formula: the small-angle differential cross section for elastic scattering, the probability distribution for the primary scattering angle β, and the energy-transfer integral for the secondary collision with scattering angle θ.

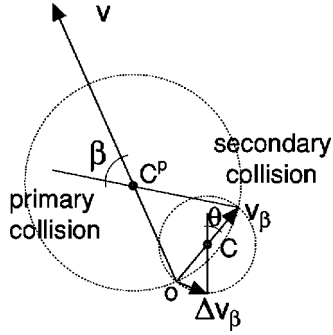[1] Joint institute of the National Institute of Science and Technology and the University of Colorado, Boulder, CO.

FIG. 2. Newton diagram in velocity space of primary and secondary collisions. The origin of the laboratory system is O; the origin of the center-of-mass system for primary and secondary collisions is indicated by C^p and C, respectively. The dashed circles indicate the elastic scattering sphere of the target atom for both collisions, centered at C^p and C, respectively. The background-gas atom with velocity v transfers a velocity v_β to a trapped alkali-metal atom. Before leaving the trap, this atom, with a kinetic energy $E_\beta = \frac{1}{2}mv_\beta^2$ larger than the trap depth $\mathcal{E}$, can collide with another trapped alkali-metal atom. When the corresponding transfer $\Delta E_\beta = \frac{1}{2}m(\Delta v_\beta)^2$ of the kinetic energy is less than the trap depth $\mathcal{E}$, this secondary collision will contribute to a heating of the trap population.

A. Total-energy input

A detailed picture of primary and secondary collisions is given in Fig. 2, using a Newton diagram in velocity space [10]. In a primary collision, the particle from the background gas with energy $E_b = k_B T_b$ [4] and velocity v collides with a cold alkali-metal atom. This results in a scattering angle β in the center-of-mass system, with C^p as the origin. All scattering events result in a velocity of the target atom on the elastic scattering sphere, centered at C^p. In the laboratory system with O as origin, the transferred kinetic energy is equal to $E_\beta = \frac{1}{2}mv_\beta^2$, with $v_\beta = (\mu^p/m)\ \beta v$ in the limit of small scattering angles. Here, μ^p is the reduced mass of the primary collision system. When necessary, a superscript p is used to indicate that the parameter refers to a *primary* collision, e.g., as is the case for μ^p and C^p. When the transferred energy E_β is less than the trap depth $\mathcal{E}$, the scattered alkali-metal atom will not leave the trap and contribute to heating of the trap population. When E_β is larger than the trap depth $\mathcal{E}$, the scattered alkali-metal atom still has a finite chance for a secondary collision with another trapped alkali-metal atom, due to the finite value of the column density $\langle nl \rangle$ of the trap.

For this secondary collision we assume a scattering angle θ in the corresponding center-of-mass system, centered at C. The transferred velocity is given by $\Delta v_\beta(\theta) = (\mu/m)\theta v_\beta$ (assuming small-angle scattering) with m the mass of the atoms in the trap and μ the reduced mass of the secondary collision system. For energies $\Delta E_\beta(\theta) = \frac{1}{2}m(\Delta v_\beta)^2$ less than the trap depth $\mathcal{E}$, these secondary collisions will lead to heating of the trap population. Of course, the primary collision rate $\dot{\mathcal{N}}$ is the driving force of the heating by secondary collisions.

The energy input $\dot{U}$ per second to the total number N of trapped atoms is then given by

$$\dot{U} = \dot{\mathcal{N}} \int_{\beta_{max,b}}^{\pi} P(\beta)d\beta$$

$$\times \langle nl \rangle \int_{0}^{\theta_{max,\beta}} \sigma_\beta(\theta)\Delta E_\beta(\theta)2\pi \sin\theta d\theta,$$

$$= \dot{\mathcal{N}}\langle nl \rangle \int_{\beta_{max,b}}^{\pi} d\beta\, P(\beta)\mathcal{I}_{QE,\beta}, \qquad (1)$$

with $P(\beta)d\beta$ the probability distribution for a primary collision with a scattering angle β. A subscript b or β is used to indicate the kinetic energy E_b and E_β, respectively, to which the specific parameter relates. The first integral of the primary collisions extends from the maximum scattering angle $\beta_{max,b}$ to π, i.e., treats all product alkali-metal atoms with an energy transfer $E_\beta \geq \mathcal{E}$.

The second integral in the first line of Eq. (1) is the energy-transfer integral for the secondary collisions with an energy E_β in the laboratory system [4]. The product of the column density $\langle nl \rangle$ and the differential cross section $\sigma_\beta(\theta)$ at energy E_β determines the finite chance for a secondary collision before leaving the trap, with a corresponding energy transfer $\Delta E_\beta(\theta)$. The second integral extends over the range 0 to $\theta_{max,\beta} = (m/\mu)(\mathcal{E}/E_\beta)^{1/2}$, with the upper limit corresponding to an energy transfer $\Delta E_\beta(\theta_{max,\beta}) = \mathcal{E}$. In this integral we include all the products of secondary collisions that remain trapped.

In the second line of Eq. (1) we have introduced the shorthand notation $\mathcal{I}_{QE,\beta}$ for the energy-transfer integral at energy E_β. We will now investigate the separate factors in this equation.

B. Small-angle differential cross section $\sigma(\theta)$

The long-range atom-atom interaction is well described by an inverse power-law potential $V(R) = C_6/R^6$ for induced dipole-dipole interaction. For our calculation of both the alkali-metal-atom–background-gas primary collisions as well as the alkali-metal-atom–alkali-metal-atom secondary collisions, we use an accurate semiempirical representation [11] of the small angle differential cross section $\sigma(x)$ at a scattering angle x. This function is given by

$$\mathcal{F}(x^*) = \sigma(x)/\sigma(0)$$

$$= \{1 - 3.75\sin(0.556x^{*2}) + 2.94x^{*2}\}^{-7/6}, \quad (2)$$

$$x^* = x/x_0 = x/(4\pi/k^2 Q)^{1/2}, \qquad (3)$$

with x^* a scaled scattering angle and $x_0 = (4\pi/k^2 Q)^{1/2}$ the characteristic diffraction angle [9–13], with $k = \mu v/\hbar$ the wave number and Q the total cross section. The asymptotic behavior of this model function is in excellent agreement with the quantum-mechanical prediction for diffraction-dominated scattering at small angles $x^* \ll 1$ and the classical or high-energy approximation at large angles $x^* \gg 1$. The function $\mathcal{F}(x^*)$ is shown in Fig. 3, together with the refractive limit $0.284x^{*-7/3}$ corresponding to classical mechanics for $x^* \gg 1$. The model function of Eq. (2) is correctly normalized: the integral $\int_0^\infty \sigma(x)2\pi \sin x dx \approx \int_0^\infty \sigma(x)2\pi x dx$
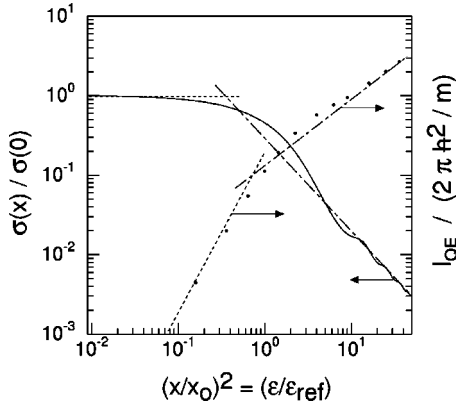
FIG. 3. Small-angle differential cross section $\sigma(x)/\sigma(0)$ for the case of a C_6/R^6 potential for atom-atom thermal collisions with scattering angle x, as a function of the scaled scattering angle $(x/x_0)^2$. Full curve: quantum-mechanical calculations; dotted line: diffractive approximation; dash-dotted line: classical mechanics. On the same scale, we also show the energy-transfer integral $\mathcal{I}_{QE}$ as a function of the scaled trap depth $\mathcal{E}/\mathcal{E}_{\text{ref}}=(x/x_0)^2$. Data points: numerical result [Eq. (6)]; dotted line: diffractive approximation [Eq. (9)]; dash-dotted line: classical approximation [Eq. (10)].

$=2\pi x_0^2\sigma(0)\int_0^\infty \mathcal{F}(x^*)x^*dx^*=1.002Q$ gives an accurate value for the total cross section Q when using the small-angle approximation $\sin x\approx x$.

The model function of Eq. (2) will be used for calculating the probability distribution $P(\beta)d\beta$ for primary collisions in Sec. II C and for the energy-transfer integral $\mathcal{I}_{QE,\beta}$ for secondary collisions in Sec. II D. In both cases, it will be advantageous to use the scaled scattering angle $x^*=\beta^*$ for primary collisions and $x^*=\theta^*$ for secondary collisions.

C. Probability distribution $P(\beta)$

The probability distribution function for the primary collisions with scattering angle β in Eq. (1) is given by (see the Appendix)

$$P(\beta)d\beta=\sigma_b^p(\beta)2\pi\sin\beta d\beta/Q_b^p. \quad (4)$$

Here σ_b^p and Q_b^p are the differential cross section and total cross section, respectively, for *primary* collisions (superscript p) at kinetic energy $E_b=k_BT_b$ of the impinging background gas atom (subscript b). By substituting the model function $\mathcal{F}$ of Eq. (2) for the differential cross section, Eq. (4) can be written as

$$P(\beta)d\beta\approx[2\pi\beta_{0,b}^2\sigma_b^p(0)/Q_b^p]\mathcal{F}(\beta^*)\beta^*d\beta^*$$
$$=0.764\mathcal{F}(\beta^*)\beta^*d\beta^*, \quad (5)$$

switching to the scaled variable $\beta^*=\beta/\beta_{0,b}$, with $\beta_{0,b}$ the characteristic diffraction angle of the primary collision at energy E_b. By using the relations of the Appendix we find the final expression of Eq. (5), which can be readily applied for numerical and analytical calculations.

D. Energy-transfer integral

The essential input for the calculation of the energy transfer rate by secondary collisions is the energy-transfer integral $\mathcal{I}_{QE,\beta}$, i.e., the integral of the product of the differential cross section at energy E_β and the associated energy transfer in the laboratory system [Eq. (1)]. Using the model function for the differential cross section given in Eq. (2), we can write the energy-transfer integral as [4]

$$\mathcal{I}_{QE,\beta}=0.764(2\pi\hbar^2/m)\int_0^{\theta_{max,\beta}^*}\mathcal{F}(\theta^*)\theta^{*\,3}d\theta^*, \quad (6)$$

$$\theta_{max,\beta}^*=(\theta_{max,\beta}/\theta_{0,\beta})=(\mathcal{E}/\mathcal{E}_{\text{ref},\beta})^{1/2}. \quad (7)$$

The scaling factor of the integral in Eq. (6) depends only on the mass m of the target atom. The dependency on the energy E_β only enters through the upper limit $\theta_{max,\beta}^*$ of the integral, as expressed in terms of the parameter $\mathcal{E}_{\text{ref},\beta}$. The latter parameter is a reference value for the depth $\mathcal{E}$ of the trap, which determines the transition from heating to trap-loss collisions. The reference value has been introduced in a recent paper by Beijerinck [4], and is defined as

$$\mathcal{E}_{\text{ref},\beta}=E_\beta\theta_{0,\beta}^2(\mu/m)^2. \quad (8)$$

The reference value depends on the initial kinetic energy, both directly by the factor E_β and implicitly by the dependency of the diffraction angle $\theta_{0,\beta}$ on E_β. Through $\theta_{0,\beta}$, the reference value also depends on the reduced mass μ and the interaction strength C_6 [4] of the collision system, in this case the secondary collisions of the alkali-metal atoms in the trap.

For the limiting cases of pure diffractive scattering (quantum regime) or pure refractive scattering (classical mechanics), the dimensionless integral in Eq. (6) can be evaluated analytically. We then find the asymptotic results [4]

$$\theta_{max,\beta}^{*2}\ll 1: \quad \mathcal{I}_{QE,\beta}\approx 0.191(2\pi\hbar^2/m)(\mathcal{E}/\mathcal{E}_{\text{ref},\beta})^2, \quad (9)$$

$$\theta_{max,\beta}^{*2}\gg 1: \quad \mathcal{I}_{QE,\beta}\approx 0.131(2\pi\hbar^2/m)(\mathcal{E}/\mathcal{E}_{\text{ref},\beta})^{5/6}, \quad (10)$$

with $\theta_{max,\beta}^{*2}$ defined in Eq. (7). Here we directly see the application of the reference value to obtain simple analytical formula for the energy-transfer integral. The two asymptotic expressions are plotted in Fig. 3, where they are compared to the numerical results for $\mathcal{I}_{QE,\beta}$ as calculated using Eq. (6). The deviations are only minor. We can therefore apply the analytical results of Eqs. (9) and (10) to evaluate the expression for the total-energy input to the trapped atoms, as given in Eq. (1).

III. TOTAL-ENERGY INPUT: SCALING LAWS

The energy-transfer integral $\mathcal{I}_{QE,\beta}$ at energy E_β [Eq. (1)] depends on the scattering angle β: only by a careful investigation of the scaling properties of the energy-transfer integral $\mathcal{I}_{QE,\beta}$ with the collision parameters can we avoid a messy approach which ends only in numerical results. Our

TABLE I. System parameters for the alkali-metal–background-gas and like alkali-metal–alkali systems, together with the diffraction angle and the scaling value for the trap depth at energy $E_b/k_B = 300$ K. For the background gas we have chosen rare-gas atoms that are usually abundant in an ion-getter-pumped ultrahigh-vacuum system: He, Ne, and Ar.

		Li	Na	K	Rb	Cs
Like alkali metals	m(a.u.)	7	23	39	87	133
	C_6(a.u.)[a]	1393.4	1556	3897	4691	6851
	$\theta_{0,b}$ (mrad)	24.6	11.8	7.1	4.3	3.1
	$\mathcal{E}_{\mathrm{ref},b}$ (mK)	45.4	10.4	3.83	1.36	0.702
He	C_6(a.u.)[b]	21.8	24.1	34.1	36.8	42.5
	$\beta_{0,b}$ (mrad)	62	45.5	40	37	36
	$\mathcal{E}^p_{\mathrm{ref},b}$ (mK)	268	78.4	40.2	17.5	10.8
Ne	C_6(a.u.)[b]	42.6	47.0	66.3	71.7	82.7
	$\beta_{0,b}$ (mrad)	51	24.1	18.2	14.6	13.3
	$\mathcal{E}^p_{\mathrm{ref},b}$ (mK)	149	43.5	22.4	9.7	6.0
Ar	C_6(a.u.)[b]	170.5	188.7	268.7	290.9	336.3
	$\beta_{0,b}$ (mrad)	44	17.7	12.2	8.6	7.5
	$\mathcal{E}^p_{\mathrm{ref},b}$ (mK)	74.3	21.7	11.1	4.8	3.0

[a]Reference [19].
[b]Reference [20].

aim is to provide analytical expressions which will give us insight into the role of secondary collisions.

A. Scaling of $\mathcal{I}_{QE,\beta}$

We first investigate the scaling properties of the energy-transfer integral $\mathcal{I}_{QE,\beta}$ for secondary collisions at a kinetic energy E_β. In terms of the primary collisions parameters, the kinetic energy E_β is equal to

$$E_\beta = \mathcal{E}^p_{\mathrm{ref},b}\beta^{*\,2}, \tag{11}$$

$$\mathcal{E}^p_{\mathrm{ref},b} = E_b\beta^2_{0,b}(\mu^p/m)^2(m/m^p). \tag{12}$$

The parameter $\mathcal{E}^p_{\mathrm{ref},b}$ is the scaling parameter for the primary collisions with background-gas atoms with a kinetic energy E_b, mass m^p, and reduced mass μ^p [4]. As usual, $\beta^* = \beta/\beta_{0,b}$ is the scaled scattering angle of the primary collision.

Using the relations of the Appendix, we can write the reference value $\mathcal{E}_{\mathrm{ref},\beta}$ for secondary collisions at a collision-angle dependent-energy E_β in terms of a reference value for secondary collisions at a fixed energy. For simplicity, we choose the kinetic energy of the primary collision, E_b, as the fixed energy for the scaling of the reference value of the secondary collision. The result reads

$$\mathcal{E}_{\mathrm{ref},\beta} = \mathcal{E}_{\mathrm{ref},b}(E_\beta/E_b)^{1/5} = \mathcal{E}_{\mathrm{ref},b}(\mathcal{E}^p_{\mathrm{ref},b}/E_b)^{1/5}\beta^{*\,2/5}. \tag{13}$$

The first step of Eq. (13) shows the simple scaling of the reference value for the secondary collision system with the kinetic energy. By substituting the result of Eq. (11) for E_β, we obtain the final result. The kinetic-energy dependency of the reference value $\mathcal{E}_{\mathrm{ref},\beta}$ of the secondary collision is now expressed in the factor $\beta^{*\,2/5}$ of the primary collision scat-

tering angle. The details of the secondary collision are represented by the reference value $\mathcal{E}_{\mathrm{ref},b}$, calculated at a *fixed* kinetic energy E_b.

In Eq. (13) we observe that the value of $\mathcal{E}_{\mathrm{ref},\beta}$ decreases with decreasing energy E_β of the secondary collisions. For trapped atoms with a strong long-range interaction, as is the case for the heavy alkali-metal–alkali-metal systems Rb and Cs, the value of $\mathcal{E}_{\mathrm{ref},b}$ at room temperature is on the order of 1 mK or less (Table I). For secondary collisions at a much lower energy, for example $E_\beta = 1$ K, the reference value $\mathcal{E}_{\mathrm{ref},\beta}$ is on the order of 300 μK or less. Even for shallow traps this already results in a maximum secondary collision angle in the range of classical scattering, as determined by the condition $\theta^{*\,2}_{max,\beta} = (\mathcal{E}/\mathcal{E}_{\mathrm{ref},\beta}) \geqslant 1$. This implies that we can use the analytical result of Eq. (10) for the energy transfer integral $\mathcal{I}_{QE,\beta}$. Using Eq. (11) for the scaling of $\mathcal{E}_{\mathrm{ref},b}$ we then find a simple result for the scaling of $\mathcal{I}_{QE,\beta}$ with the scaled primary collision angle β^*, as given by

$$\mathcal{I}_{QE,\beta} = 0.131(2\pi\hbar^2/m)(\mathcal{E}/\mathcal{E}_{\mathrm{ref},b})^{5/6}(\mathcal{E}^p_{\mathrm{ref},b}/E_b)^{-1/6}\beta^{*\,-1/3}. \tag{14}$$

In Eq. (14) the energy transfer integral at a variable energy E_β, which depends on the scattering angle β of the primary collision, is now expressed in terms of the reference values $\mathcal{E}^p_{\mathrm{ref},b}$ and $\mathcal{E}_{\mathrm{ref},b}$ at a fixed energy E_b, and the scaled scattering angle β^* of the primary collision. This allows an easy implementation in Eq. (1).

B. Energy input

The final expression for the energy input per second, $\dot{U}$, to the population of N trapped atoms [Eq. (1)] can now be

evaluated, using the results of Eqs. (4) and (14) as input. We then find[1]

$$\dot{U} = \dot{\mathcal{N}} \langle nl \rangle \left[0.131 \left(\frac{2\pi\hbar^2}{m} \right) \left(\frac{\mathcal{E}}{\mathcal{E}_{\text{ref},b}} \right)^{5/6} \left(\frac{\mathcal{E}^p_{\text{ref},b}}{E_b} \right)^{-1/6} \right]$$

$$\times \left[0.764 \int_{\beta^*_{max,b}}^{\infty} \beta^{*\ 2/3} \mathcal{F}(\beta^*) d\beta^* \right]. \tag{15}$$

The integral over the primary collisions in the range $\beta^*_{max,b}$ to ∞ can be solved numerically, using the simple but accurate expression of Eq. (4) as input. However, to obtain more insight into the scaling of the energy input $\dot{U}$ with the system parameters, we can also derive a fully analytical result. By substituting the classical approximation for the differential cross section in the weight function $P(\beta^*)d\beta^*$ in Eq. (15), we find

$$\dot{U} = \dot{\mathcal{N}} \langle nl \rangle \left[0.131 \left(\frac{2\pi\hbar^2}{m} \right) \left(\frac{\mathcal{E}}{\mathcal{E}_{\text{ref},b}} \right)^{5/6} \left(\frac{\mathcal{E}^p_{\text{ref},b}}{E_b} \right)^{-1/6} \right]$$

$$\times \left[0.328 \left(\frac{\mathcal{E}}{\mathcal{E}^p_{\text{ref},b}} \right)^{-1/3} \right]. \tag{16}$$

The second factor in square brackets in Eq. (16) corresponds to the analytical result for the integral in Eq. (15).

Combining the two factors in Eq. (16), we observe that the energy input scales as $\dot{U} \sim \mathcal{E}^{1/2}$. For the scaling with the reference value of the primary collision we find $\dot{U} \sim (\mathcal{E}^p_{\text{ref},b})^{1/6}$, i.e., only a very weak dependence. For the dependence on the reference value of the secondary collision we find $\dot{U} \sim (\mathcal{E}_{\text{ref},b})^{-5/6}$, as would be the case for the energy-transfer rate for primary collisions with alkali-metal atoms in the classical limit.

Only a small error is made when using the expression for the weight function $P(\beta^*)d\beta^*$ that corresponds to classical scattering over the full range of integration, including the range from $\beta^* = \beta^*_{max,b}$ to $\beta^* = 1$ in the quantum regime of primary collisions. When looking at the differential cross section in Fig. 3, we observe that we can expect compensating effects in this case. For angles β^* slightly larger than unity, the first diffraction oscillation in the differential cross section is larger than the classical approximation; for angles β^* slightly less than unity, the value of $\sigma(\beta^*)$ is always smaller than the classical result. These ideas have been checked by solving the integral in Eq. (15) numerically. This calculation shows that for $\beta^*_{max,b} = 0.1$ the numerical results are 53% smaller than the analytical approximation, as given in Eq. (16). For $\beta^*_{max,b} = 0.7$, the numerical results are 25% larger than the analytical approximation; this difference then decreases to a few percent in the range $2 < \beta^*_{max} < 10$.

---

[1]A dimensional check shows a factor $[\text{time}]^{-1}$ from the primary collision rate $\dot{\mathcal{N}}$ and a factor $[\text{energy}]$ from the term $\langle nl \rangle$ $(2\pi\hbar^2/m)$, in agreement with the dimension $[\text{energy/time}]$ of $\dot{U}$.

IV. ANALYTICAL RESULTS FOR ENERGY-TRANSFER RATE

With all the hard work done for calculating the energy-transfer rate for secondary collisions, we can now compare our results with the energy-transfer rate by primary collisions. The proof of the pudding is in the eating: this comparison will show us when one or the other heating mechanism will dominate. We also investigate the scaling of the calculated heating rates with the background species, the properties of the trapped alkali-metal atom and details of the trap such as the trap depth and the column density. For this comparison we will use standard conditions for both the background gas and the trapping parameters, as given by

$$\text{trap-loss lifetime:} \quad \tau^p = 100 \ \text{s},$$

$$\text{trap depth:} \quad \mathcal{E} = 1 \ \text{mK},$$

$$\text{column density:} \quad \langle nl \rangle = 10^{15} \ \text{m}^{-2}, \tag{17}$$

$$\text{background gas:} \quad \text{He at } E_b = 300 \ \text{K}, \tag{18}$$

$$\text{trap atoms:} \quad \text{Rb}. \tag{19}$$

The trap depth is typical for a magnetic trap, although on the low side. The column density corresponds to a trap with a density $n = 10^{14} \ \text{cm}^{-3}$ and a size of 10 μm, typical numbers for Rb traps just above the transition to Bose-Einstein condensation. As the driving force we assume He-Rb primary collisions, with a reference value equal to $\mathcal{E}^p_{\text{ref},b} = 17.5$ mK (Table I).

A. Primary collisions

The background gas collision partners He, Ne, and Ar are relevant for the residual gases in an ion-getter-pumped ultrahigh-vacuum system, in combination with a titanium sublimation pump. The long-range van der Waals coefficients are given in Table I, together with the corresponding diffraction angle $\beta_{0,b}$ and reference value $\mathcal{E}^p_{\text{ref},b}$ at energy $E_b/k_B = 300$ K.

For background collisions with non-alkali atoms, the trap-loss lifetime τ^p is in good approximation related to the total number of primary collisions as $\dot{\mathcal{N}}/N = 1/\tau^p$. The small fraction $\Delta Q^p_b/Q^p_b$ of the total cross section for primary collisions, that results in heating but not in traploss, is equal to $\Delta Q^p_b/Q^p_b = 0.38(\mathcal{E}/\mathcal{E}^p_{\text{ref},b})$ [4]. For the He-Rb system we find $(\mathcal{E}/\mathcal{E}^p_{\text{ref},b}) = 0.09$, resulting only in a 4% error in our approximation for the trap-loss lifetime.

The energy-transfer rate of secondary collisions has to be compared to the density-independent energy-transfer rate $\dot{U}^p/N$ due to primary collisions [4]. For an easy comparison, we write the primary-collision energy-transfer rate as [4]

$$\left(\frac{\dot{U}^p}{Nk_B} \right) = 110 \ \text{nK/s} \times \left(\frac{100 \ \text{s}}{\tau^p} \right) \left(\frac{\mathcal{E}}{1 \ \text{mK}} \right)^2 \left(\frac{\mathcal{E}^p_{\text{ref},b}}{17.5 \ \text{mK}} \right)^{-1}. \tag{20}$$

This result holds for the quantum regime of primary collisions with $\beta_{max,b}^{*2} = \mathcal{E}/\mathcal{E}_{ref,b}^p < 1$. Here the numerical factor 110 nK/s is equal to the primary-collision energy-transfer rate for He-Rb background collisions at the standard conditions of Eq. (19).

B. Secondary collisions

For the numerical value of the energy transfer rate $\dot{U}/N$ for secondary collisions, we find [using Eq. (16)]

$$\left(\frac{\dot{U}}{Nk_B}\right) = 153 \quad \text{nK/s} \times \left(\frac{100 \ \text{s}}{\tau^p}\right)\left(\frac{\langle nl \rangle}{10^{15} \ \text{m}^{-2}}\right)\left(\frac{87}{M}\right)$$

$$\times \left(\frac{\mathcal{E}}{1 \ \text{mK}}\right)^{1/2}\left(\frac{\mathcal{E}_{ref,b}}{1.36 \ \text{mK}}\right)^{-5/6}\left(\frac{\mathcal{E}_{ref,b}^p}{17.5 \ \text{mK}}\right)^{1/6}$$

$$\times \left(\frac{E_b}{300 \ \text{K}}\right)^{1/6}. \tag{21}$$

The numerical factor 200 nK/s is the energy transfer rate for secondary Rb-Rb collisions for a trap at the standard conditions of Eq. (19).

Looking at Eq. (20), we observe that the energy-transfer rate by primary collisions has a steeper dependency $\dot{U}^p/N \sim \mathcal{E}^2$ on the trap depth than observed in the energy-transfer rate $\dot{U}/N \sim \mathcal{E}^{1/2}$ by secondary collisions [Eq. (21)]. This implies that, for decreasing values of $\mathcal{E}$, there always is a crossover point $\mathcal{E}_X$ where heating by secondary collisions is equal to heating by primary collisions. Comparison of Eq. (20) with Eq. (21) shows a crossover point at $\mathcal{E}_X = 1.25$ mK where, with decreasing trap depth, heating by secondary Rb-Rb collisions takes over from heating by primary He-Rb collisions. Once we are in the regime $\mathcal{E} < \mathcal{E}_X$, simply lowering the trap depth is not a very efficient means to reduce the energy-transfer rate, due to the $\mathcal{E}^{1/2}$ dependency of heating by secondary collisions.

C. Rb−rare-gas collisions

We will now investigate the energy-transfer rate for secondary collisions in more detail. In Fig. 4 we show the results for Rb as a function of the trap depth $\mathcal{E}$, for all different primary collision partners He through Ar. For this calculation we have used the standard conditions as given in Eq. (19). The general trend is the same for all collision partners. This can be directly understood from the weak $(\mathcal{E}_{ref,b}^p)^{1/6}$ dependency on the collision properties of the background gas. For comparison we have also depicted the trap-density-independent energy-transfer rate $\dot{U}^p/N$ for primary collisions [Eq. (20)]. In all cases, we again observe that the energy-transfer rate for secondary collisions crosses the primary-collision energy transfer rate in the quantum regime of primary scattering angles.

In Fig. 5 we depict the energy-transfer rate as a function of the column density $\langle nl \rangle$, calculated with the analytical approximation of Eq. (16) at the standard conditions of Eq. (19) with the exception of the trap depth $\mathcal{E}$. Results are given
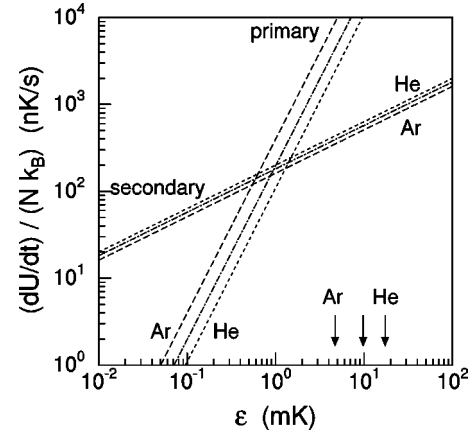

FIG. 4. Energy-transfer rate $\dot{U}/N \sim \mathcal{E}^{1/2}$ by secondary collisions for Rb as a function of the trap depth $\mathcal{E}$, for the background gases He, Ne, and Ar. For the column density and the trap-loss lifetime of the trap, we have used the standard values $\langle nl \rangle = 10^{15}$ m^{-2} and $\tau^p = 100$ s, respectively. For comparison, we have also drawn the energy-transfer rate due to primary collisions. The arrows indicate the transition from diffractive scattering (slope 2) to classical scattering (slope 5/6) for $\mathcal{E} \approx \mathcal{E}_{ref,b}^p$. With decreasing value of $\mathcal{E}$ we observe a crossover from the primary-collision energy-transfer rate to the secondary-collision energy-transfer rate.

for a background gas of He for two different values of the trap depth. For comparison we also give the value of the trap-density-independent energy-transfer rate due to primary collisions. Due to the different scaling of both contributions with trap depth, the crossing point $\mathcal{E}_X$ shifts from a high column density $\langle nl \rangle = 5 \times 10^{14}$ m^{-2} for $\mathcal{E} = 1.0$ mK to a low column density $\langle nl \rangle = 5 \times 10^{13}$ m^{-2} for $\mathcal{E} = 0.2$ mK.

In Fig. 6 we have plotted the energy-transfer rate $\dot{U}/N$ for the alkali-metal atoms Li through Cs as a function of the trap depth $\mathcal{E}$, for the standard conditions of Eq. (19). The rate is calculated in the analytical approximation of Eq. (16). We
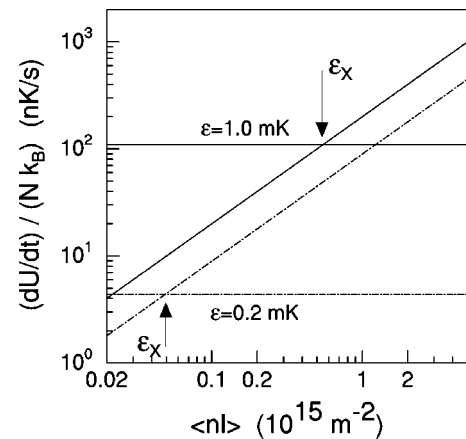

FIG. 5. Energy-transfer rate $\dot{U}/N$ for a Rb trap, plotted as a function of the column density $\langle nl \rangle$. Results are given for He as a background gas, for two values $\mathcal{E} = 1.0$ and 0.2 mK of the trap depth. In both cases a trap-loss lifetime $\tau^p = 100$ s is assumed. For comparison the energy-transfer rate by primary collisions is given as a horizontal line, together with the crossover point $\mathcal{E}_X$.
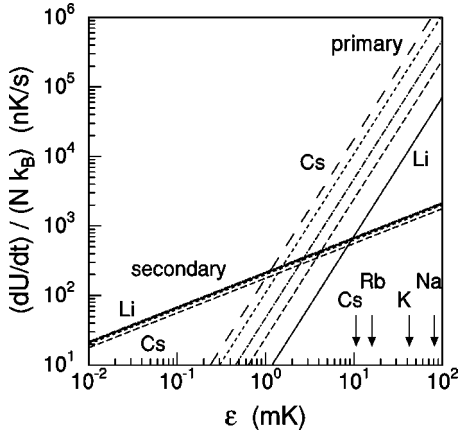
FIG. 6. Energy-transfer rate $\dot{U}/N$ for the alkali-metal atoms Li through Cs as a function of the trap depth $\mathcal{E}$, assuming He as the background gas. For the column density and the particle loss lifetime of the trap we have used the standard value $\langle nl\rangle = 10^{15}$ m^{-2} and $\tau^p = 100$ s, respectively. The arrows indicate the transition point for primary collisions from diffractive scattering (slope 2) to classical scattering (slope 5/6), which is located at $\mathcal{E} \approx \mathcal{E}_{\mathrm{ref},b}^p$.

have also plotted the energy-transfer rate by primary collisions. The arrows indicate the crossover point for primary collisions from the quantum regime to the classical regime of collisions [Eq. (3)]. For all systems, we again observe a crossover with the direct energy-transfer rate in the quantum regime of primary collisions. The maximum primary-collision scattering angles at the crossover $\mathcal{E}_X$ are equal to $\beta_{max,b}^* = 0.19$ to 0.32 for Li through Cs, respectively, well into the quantum range of scattering.

The system dependency of the value of $\mathcal{E}_X$ is determined mainly by the system dependency of the heating rate by primary collisions. The dependency of the energy-transfer rate by secondary collisions on the specific alkali-metal atom considered is only very weak. The two factors in Eq. (21) that depend on the secondary collision system, i.e., the mass factor $(87/M)$ and the reference parameter factor $(\mathcal{E}_{\mathrm{ref},b})^{-5/6}$,

surprisingly cancel out nearly all influence on the secondary energy transfer rate.

V. EFFECTIVE TRAP DEPTH $\mathcal{E}_{\mathrm{eff}}$

Until now, we have defined heating collisions as those collisions that leave an initially cold atom with a transferred energy less than the trap depth $\mathcal{E}$. Using this definition, we implicitly assume that these collisionally heated atoms will all rapidly thermalize with the sample of cold atoms, resulting in an equilibrium heating rate. However, typical sample temperatures are in the $1-40$ μK range, while the depth of the magnetic trap is on the order of $5-10$ mK. Furthermore, the collisionally heated atoms in the mK range occupy a volume that is much larger than the sample volume and their density is correspondingly low. The assumption of a rapidly developing equilibrium thus needs further refinement.

A. Oort cloud

The low-density cloud of collisionally heated but still trapped atoms was called the ''Oort cloud'' by Cornell *et al.* [8], in analogy to the extremely disperse and essentially undetectable cloud of comets located far outside the orbit of Pluto but still belonging to the solar system as proposed by Oort [14]. There is considerable experimental evidence that the mK Oort cloud does exist. In the low-temperature range of the sample of trapped atoms, at the end of the evaporative cooling cycle, the total population of the Oort cloud can even exceed the population of the centrally located sample by a factor 4. Typical experimental data for the Oort cloud are given in Table III, as measured at JILA [7].

We propose a concept for the Oort cloud, where its population consists *only* of atoms with a kinetic energy E in the range $\mathcal{E}_{\mathrm{eff}} < E < \mathcal{E}$. In this concept, the Oort cloud does not contain any atoms with a kinetic energy $E \leq \mathcal{E}_{\mathrm{eff}}$. The value of $\mathcal{E}_{\mathrm{eff}}$ will be much smaller than the trap depth, but still much larger than the thermal energy of the atoms in the cold sample at the center of the trap (Fig. 7).

TABLE II. Calculated energy-transfer rate $\dot{U}/Nk_B$ for secondary collisions [Eq. (21)], in comparison with the measured values (both with and without an rf shield) of Myatt for the ^{87}Rb experiment at JILA. The calculated energy-transfer rate $\dot{U}^p/Nk_B$ for primary collisions [Eq. (20)] is given as a reference. Both the dependency on the background gas and the cutoff value $\mathcal{E}_{\mathrm{eff}}$ are given. The trap parameters used as input for the model calculation are the experimental data $\langle n\rangle = 3\times10^{13}$ cm^{-3}, $T = 1.2$ μK, $\omega_r/2\pi = 110$ Hz, and $\tau^p = 250$ s, resulting in $l_r = 15.5$ μm and $\langle nl\rangle = 1.3\times10^{15}$ m^{-2}.

	Background	No shield $\mathcal{E}_{\mathrm{eff}} = 200$ μK	400 μK	rf shield 48 μK
Secondary collisions	He	35 nK/s	50 nK/s	17 nK/s
	Ar	29 nK/s	40 nK/s	14 nK/s
	Rb	22 nK/s	31 nK/s	11 nK/s
Primary collisions	He	1.8 nK/s	7.2 nK/s	0.1 nK/s
	Ar	6.4 nK/s	26 nK/s	0.4 nK/s
	Rb	31 nK/s	126 nK/s	1.8 nK/s
Experimental[a]		120 nK/s		60 nK/s

[a]Myatt [7].

TABLE III. Input parameters for the calculation of the heating of the sample in the center of the trap by collisions with atoms in the Oort cloud, together with the resulting energy-transfer rate as calculated for two different values of the cutoff energy $\mathcal{E}_{\text{eff}}$. The numbers are typical for trapped samples of Rb atoms at JILA.

parameter	value[a]
T_{Oort}	2 mK
N_{Oort}/N	1–4
N	$5 \times (10^5 - 10^6)$
V_{Oort}	$\approx 10^{-1}$ cm^3
n_{Oort}	5×10^5 cm^{-3} [b]
v_{Oort}	76 cm/s
$\mathcal{E}_{\text{ref,Oort}}$	125 μK
$\mathcal{E}_{\text{eff}} = 48$ μK	7 nK/s[b]
$\mathcal{E}_{\text{eff}} = 200$ μK	25 nK/s[b]
$\mathcal{E}_{\text{eff}} = 400$ μK	45 nK/s[b]

[a]Myatt [7].
[b]Lower limit $N_{\text{Oort}} = 5 \times 10^5$.

The parameter $\mathcal{E}_{\text{eff}}$ serves as an effective cutoff for the energy-transfer integral. We assume that primary and secondary collisions with an energy transfer *larger* than $\mathcal{E}_{\text{eff}}$ but less than $\mathcal{E}$ are lost in the Oort cloud: this constitutes an effective-loss mechanism for atoms in the cold sample at the center of the trap. Collisions with an energy transfer larger than $\mathcal{E}$ actually escape from the trap. In both cases these atoms do not contribute to the energy-transfer rate to the cold sample in the center of the trap.

Conversely, primary and secondary collisions with an energy transfer *less* than $\mathcal{E}_{\text{eff}}$ *do* contribute to heating of the cold sample in the center of the trap, due to a rapid thermalization in a series of collisions. By intuition, we expect that the value of $\mathcal{E}_{\text{eff}}$ will at maximum be one or two orders of magnitude larger than the temperature of the cold sample in the center of the trap, i.e., in the range of hundreds of μK. For a comparison of our model calculations with experimental results in Sec. VII, we use extreme values of the range
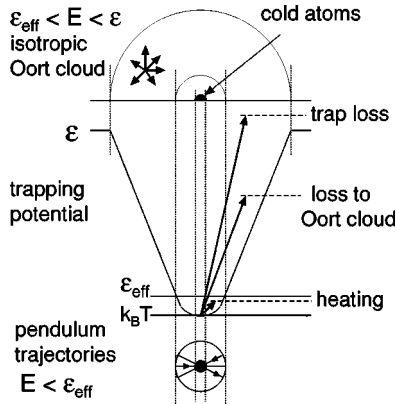

FIG. 7. Schematic of the trapping potential, the Oort cloud, and the region of rapid thermalization by ''pendulum'' trajectories of the products of secondary collisions with a transferred kinetic energy less than the cutoff $\mathcal{E}_{\text{eff}}$.
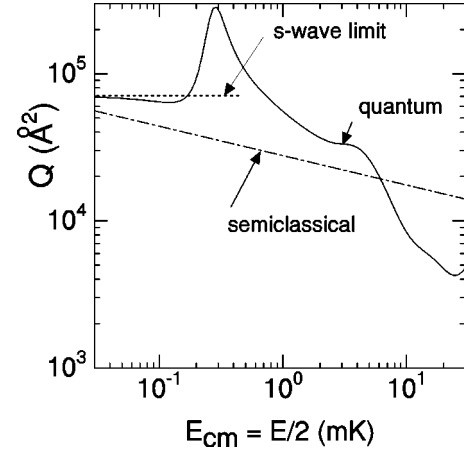

FIG. 8. Total cross section for elastic ^{87}Rb$+ ^{87}$Rb collisions in the $|1,-1\rangle$ state, as a function of the center-of-mass energy $E_{cm} = E/2$. Both the fully quantum-mechanical results (with contributions for $l = 0$, 2, 4, and 6) as well as the semiclassical formula of Eq. (A1) are given. The range of validity of the latter expression starts when five to ten angular momenta contribute, at a center-of-mass energy $E_{cm} = 5 - 20$ mK.

$$200 \ \mu\text{K} \leqslant \mathcal{E}_{\text{eff}} \leqslant 400 \ \mu\text{K} \qquad (22)$$

to test our new concept of the Oort cloud in trap heating. This comparison can help us to fix a value for $\mathcal{E}_{\text{eff}}$ which is most realistic.

An important conclusion of this new concept of heating collisions is evident when we look at Fig. 4. The value for $\mathcal{E}_X$, the transition point from dominant heating by secondary collisions to dominant heating by primary collisions, is always larger than the proposed value for the cutoff, as given in Eq. (22). We can conclude that we are *always* in the regime where heating by secondary collisions is the dominant mechanism, proportional to the column density of the trap. A second important conclusion is that the experimentally observed heating rates do not depend on the actual trap depth $\mathcal{E}$, at least when the latter is larger than, e.g., 1 mK. For shallow traps with a depth < 1 mK, the formation of an Oort cloud is not to be expected.

B. Thermalizing collisions

To investigate the validity of our assumption of a rapid thermalization for atoms with a kinetic energy less than $\mathcal{E}_{\text{eff}}$, we discuss a ''pendulum model'' for the interaction of collisionally heated atoms with the cold sample in the center of the trap. In this model, we assume that all these atoms have a negligible macroscopic angular momentum in the trap. This implies that these collisionally heated atoms traverse the cold sample in the center of the trap *twice* per oscillation period (Fig. 7). At each crossing, the probability for a collision is equal to $[1 - \exp(-\langle nl \rangle Q)]$, with Q the total cross section. For a kinetic energy $E \leqslant 400$ μK we can use the s-wave limit $Q_{T \to 0}$ for the total cross section (Fig. 8). The time constant $\tau_{thermal}$ for the thermalization of a collisionally heated atom to the trap temperature is then given by

$$\tau_{thermal}^{-1} = (\omega/\pi)\langle nl\rangle Q_{T\to 0}, \tag{23}$$

with ω the angular frequency of the atom trap in the coordinate of tightest confinement, i.e. the largest frequency.

For Rb, the single-crossing collision probability is equal to $\langle nl\rangle Q_{T\to 0} = 0.50$ for a typical value of 10^{15} m^{-2} for the column density. On the average, half of the kinetic energy of the collisionally heated atom is transferred in each collision to the cold atom in the trap, due to the isotropic nature of s-wave collisions. For example, a 100-μK atom will thermalize to a temperature of 1 μK in typically seven collisions, i.e. in a time span approximately equal to 7 $\tau_{thermal}$ = 54 ms when inserting a typical experimental value $\omega/2\pi$ = 150 Hz. This collision time should be compared to typical values for the elastic collision time in the cold sample in the center of the trap, which ranges from 3 to 100 ms [7].

Although all collisionally heated atoms that are still trapped originate from a collision with an atom in the sample at the center of the trap, the assumption that they will follow a pendulum movement is most appropriate for low-energy atoms. These atoms probe the low-energy region of the trap, where the absolute value of the anisotropy of the trapping potential is small. With increasing kinetic energy, the atoms will probe the more anisotropic region of the trap, and acquire a larger macroscopic angular momentum. These atoms will circle around the sample in the center of the trap rather then hitting it twice per period of oscillation. The latter atoms do not thermalize rapidly and are lost in the Oort cloud. The cutoff energy $\mathcal{E}_{eff}$ is the transition from one regime to the other.

VI. COLUMN DENSITY OF TRAP

Before we can compare our model with experimental results, we have to give a clear definition of the average value $\langle nl\rangle$ of the column density. We assume a Boltzmann distribution for the density profile in both the axial and radial directions. Integration over the Gaussian density profile in radial direction shows that the effective "density-length" product for a cigar-shaped harmonic trap with trapping frequencies $\omega_r \ll \omega_z$ is, in a good approximation equal to

$$\langle nl\rangle = 0.886(\pi/2)n(0)l_r, \tag{24}$$

with $n(0)$ the peak value of the density and $l_r = (k_B T/m\omega_r)^{1/2}$ the rms radius of the trap population. The factor $\pi/2$ stems from the fact that the solid-angle-weighted average path in a three-dimensional trap is a factor $\pi/2$ larger than the distance traveled in the radial direction [15].

For a direct comparison with the expression given by Myatt, we also write Eq. (24) as a function of the density-weighted average value $\langle n\rangle$ of the density, resulting in

$$\langle nl\rangle = 2.50(\pi/2)\langle n\rangle l_r,$$

$$\langle n\rangle = N^{-1}\int\int\int n^2(\vec{r})d^3\vec{r} = n(0)/2^{3/2}. \tag{25}$$

The result in Eqs. (25) differs by a factor $(2.50/\pi^{1/2}) = 1.41$ from the expression $\langle nl\rangle = (\pi^{3/2}/2)\langle n\rangle l_r$ given by Myatt [7].

Clearly, this difference of a factor $2^{1/2}$ in the work of Myatt is the result of applying the model of an *infinitely* long trap in axial direction, which results in a different relation $\langle n\rangle_{2D} = n(0)/2$ between the average value of the density and the peak density. For a full three-dimensional (3D) approach the relation between the peak density and the average value reads $\langle n\rangle_{3D} = n(0)/2^{3/2}$, as can be expected from a Gaussian profile in all three directions. The result of Eq. (24), in terms of the peak density, has the advantage that it does not depend on the specific model used for the trap geometry.

VII. COMPARISON TO ^{87}Rb EXPERIMENTS

A. Experimental results

Accurate and well-documented data on heating rates in Rb traps were given by Myatt [7] at JILA. Their first observation is the very different behavior for the two spin states $|2,2\rangle$ and $|1,-1\rangle$ that can be trapped. Typical data for a trap with average density $n = 3\ 10^{13}$ cm^{-3} and temperature $T = 1.2$ μK are heating rate of 600 and 120 nK/s for the $|2,2\rangle$ and $|1,-1\rangle$ states, respectively. Three possible reasons for the larger heating rate of the $|2,2\rangle$ state are given. First, the internal energy of the hyperfine splitting that can serve as a source of heat. Second, the existence of two trappable states in the $F = 2$ manifold, that could result in a two-step kind of heating process which can also contribute. Third, differences in the total cross section due to shape resonances for angular momenta $l \geq 2$ can have an influence on the heating rate.

The second observation of Myatt [7] is that the heating rate is proportional to the elastic collision rate γ_{el} in the sample, irrespective of the temperature and density in the trap. The experiments are not conclusive if there is a dependency on the trap frequency ω. This relationship holds both with and without applying a rf shield, over a wide range of heating rates. For example, for the $|1,-1\rangle$ spin state without a rf shield, the range of validity extends for heating rates ranging from 5 to 230 nK/s.

Their third observation is that the heating rate is strongly affected by applying an "rf shield," i.e., a rf field as used in evaporative cooling but with a cutoff temperature that is much higher than the trap temperature. For example, at $T = 1$ μK, a rf shield with a cutoff at 48 μK reduces the heating rate by a factor of 2 [7]. This "shield" will not entice atoms to leave the sample in the center, due to the vanishing population in the Boltzmann tail of the kinetic-energy distribution.

B. Model calculations

These are the facts that we have to compare with our model calculations. The first observation is outside the scope of this paper, because we only take into account single-state trapped atoms. However, we still can eliminate one of the suggestions of Myatt for explaining the observed differences. Precise calculations of the total cross section at low temperatures, as recently performed by Kokkelmans and Verhaar [16], show that there are no major differences for the two states involved. Also, both show a pronounced d-wave resonance, equally large for the $|2,2\rangle$ and $|1,-1\rangle$ states.

We now proceed to the second observation. The elastic collision rate is equal to $\gamma_{el} = \langle nQv \rangle_{trap}$, taking the average over the trap volume and the velocity distribution in the trap, respectively. When we write the average velocity as $\langle v \rangle \sim \omega_r l_r$, with l_r the typical excursion in the harmonic trap, we directly observe that the elastic collision rate is proportional to the product of trap frequency ω_r and opacity $\langle nlQ \rangle_{trap}$. For the Rb-Rb system we are in the regime of s-wave scattering when the center-of-mass energy is limited to $E_{cm} \lesssim 39 \ \mu$K, i.e., a kinetic energy of $E = 78 \ \mu$K of the trapped atoms [17]. The scaling law of Myatt for the heating rate can now be written as

$$\dot{U}/N \sim \gamma_{el} \sim \omega_r \langle nl_r \rangle Q_{T \to 0} \sim \langle nl_r \rangle, \tag{26}$$

where the last step is valid only for a fixed trapping frequency ω_r. Comparing this result to the secondary heating rate in Eq. (21) shows the same dependency on the column density when using Eq. (24) for $\langle nl \rangle$ in terms of the average density and the rms value of the radial excursion. The experiments of Myatt are not conclusive if a dependency on the radial trap frequency ω_r actually exists. Looking at the results of our model for heating by secondary collisions, the existence of such a dependency on ω_r would be rather surprising.

We now discuss the third experimental observation of Myatt. We assume that the heating rate *without* a rf shield correlates with the energy transfer by secondary collisions with a cutoff energy $\mathcal{E}_{eff}$. It is obvious that the rf shield does influence the heating by secondary collisions when the rf cutoff energy $\mathcal{E}_{rf}$ is less than the effective trap depth $\mathcal{E}_{eff}$. The decrease in heating rate when *switching on* the rf shield then corresponds to the energy transfer with an effective trap depth equal to $\mathcal{E}_{rf}$. The scaling of the energy-transfer rate by secondary collisions with $\mathcal{E}^{1/2}$ then results in a decrease in heating rate according to

$$(\dot{U}/N)_{rf} = (\mathcal{E}_{rf}/\mathcal{E}_{eff})^{1/2} (\dot{U}/N). \tag{27}$$

Considering our choice for a cutoff value in the range $200 \ \mu$K $< \mathcal{E}_{eff} < 400 \ \mu$K, the heating rate is reduced by a factor of 2–3 by applying a rf shield at a cutoff equal to $50 \ \mu$K. This reduction is of the correct order of magnitude when looking at the experimental data of Myatt.

We now look in detail at the *absolute value* of the energy-transfer rate by secondary collisions in the experiments of Myatt (Table II). In the case of a trap with density $\langle n \rangle = 3 \times 10^{13}$ cm^{-3}, temperature $T = 1.2 \ \mu$K, and trap frequency $\omega/2\pi = 110$ Hz, the column density is equal to $\langle nl \rangle \approx 1.3 \times 10^{15}$ m^{-2}; the measured trap-loss lifetime is $\tau^p \approx 250$ s. Inserting these numbers into Eq. (21), we then calculate the energy-transfer rate by secondary collisions. Results are given in Table II for two different values of the cutoff, equal to $\mathcal{E}_{eff} = 200$ and $400 \ \mu$K. By lowering the effective trap depth to $\mathcal{E}_{eff} = \mathcal{E}_{rf} = 48 \ \mu$K we can include the effect of the rf shield. For comparison we have also calculated the energy-transfer rate by primary collisions, using Eq. (20).

To show the dependency of the heating rate on the composition of the background gas, we have calculated the energy-transfer rates for three species: He, Ar, and Rb. The experimentally obtained information, showing that the energy-transfer rate nearly vanishes when extrapolating to a zero column density, helps us to decide on the composition of the background gas. A background of Rb is eliminated by its large density-independent energy-transfer rate by primary collisions, which is in strong contradiction with the column-density dependency of Myatts data [7]. The absolute value of the energy-transfer rate by secondary collisions points in the direction of He as a background gas, because it has the largest effect. Looking at the absolute values of the energy-transfer rate, we conclude that a cutoff at $\mathcal{E}_{eff} = 400 \ \mu$K gives a fair representation of the experimental results of Myatt.

Looking at the influence of the rf shield on the energy-transfer rates, the case of He and $\mathcal{E}_{eff} = 400 \ \mu$K shows a decrease of 42 nK/s when switching on the shield. This number is in fair agreement with the experimental data of Myatt, who found a decrease of ≈ 60 nK/s. However, the absolute values of the energy transfer rates with and without the rf shield are too low by approximately 30–60 nK/s, respectively.

In Sec. VIII A we will show that primary collisions with ''hot'' mK atoms in the isotropic Oort cloud could be the cause of this extra contribution. One should keep in mind that the hot atoms from the Oort cloud impinging on the cold atoms in the center of the trap are not eliminated by the rf shield: the heating collisions do not depend on the magnetic substate, at least in a first-order approximation. The influence of the rf shield is limited to the influence of the lower cutoff from heating to trap loss in these primary collisions, as reflected in the upper bound of the energy-transfer integral.

C. Background-gas composition

The scaling of the energy-transfer rate by secondary collisions with only the $(\mathcal{E}^p_{ref,b})^{1/6}$ power of the reference value of the primary collisions results in a very weak dependence on the background-gas atom. Even when switching from He-Rb primary collisions to Rb-Rb primary collisions, with $\mathcal{E}^p_{ref,b} = 17.5$ and 1.36 mK, respectively, this results in only a factor $(\mathcal{E}^{Rb}_{ref,b}/\mathcal{E}^{He}_{ref,b})^{1/6} = 0.65$ *decrease* in the predicted energy-transfer rate (Table II). This scaling is in strong contrast with the energy-transfer rate by primary collisions, which increases proportional to $(\mathcal{E}^p_{ref,b})^{-1}$ in the quantum regime of diffractive scattering (Table II).

Experimental support for this counterintuitive scaling rule, i.e., a decrease in energy-transfer rate by secondary collisions when we assume a primary collision with a much stronger long-range interaction, can also be found in the experimental work of Myatt [7]. To investigate the dependency of the heating rate on the density of the background gas, Myatt [7] heated the walls of the trapping chamber. He observed a drop in the trap-loss lifetime of his magnetic trap from $\tau^p_{cold} \approx 400$ s to $\tau^p_{hot} \approx 100$ s. Going from ''cold'' to ''hot,'' the heating rate increased by a factor 1.5 to 2.5, much less than the decrease in τ^p.

With cold walls, the background gas most likely consists of atoms with a low mass number and a weak long-range

TABLE IV. Absolute value of the heating rate in the experiment of Myatt on Rb, in comparison with the total of the three contributions by primary background collisions with He, secondary Rb-Rb collisions and primary Rb-Rb collisions with atoms in the Oort cloud, as predicted by the models in this paper [Eqs. (20), (21), and (29)].

		No shield[a]	rf shield[b]	
Model	Secondary collisions	50 nK/s	17 nK/s	$\langle nl \rangle$ dependent
	Primary collisions	7.2 nK/s	0.1 nK/s	n independent
	Oort cloud	45 nK/s	7 nK/s	n independent in first order
Model	Total heating rate	102 nK/s	24 nK/s	
Experiment	Myatt[c]	120 nK/s	60 nK/s	$\langle nl \rangle$-dependent

[a]$\mathcal{E}_{\text{eff}} = 400$ μK.
[b]$\mathcal{E}_{\text{eff}} = 48$ μK.
[c]Reference [7].

interaction, e.g., H_2, He or Ne, as shown in Sec. VII B. Heating up the chamber will result mainly in an additional flux of Rb atoms, evaporating from the walls. For the scaling of the heating rate in these two experiments, we thus have to take into account the effect of both the increase in density as well the change in composition of the background gas. For the increase in heating rate we then predict a factor

$$\frac{(\dot{U}/N)_{hot}}{(\dot{U}/N)_{cold}} = \left(\frac{\tau^p_{hot}}{\tau^p_{cold}}\right)^{-1} \left(\frac{\mathcal{E}^{\text{Rb}}_{\text{ref},b}}{\mathcal{E}^{\text{He}}_{\text{ref},b}}\right)^{1/6} = 2.6. \quad (28)$$

The good agreement with the experimental results of Myatt provides extra support for our model of heating by secondary collisions.

VIII. THERMAL COUPLING TO OORT CLOUD

In our new concept of the Oort cloud we have implicitly assumed that the Oort cloud does not contribute to the energy-transfer rate to the mK sample. However, in view of the observed discrepancies between experiments and model calculations, the latter being too small, it is necessary to investigate this assumption in more detail. We discuss two models: first, an Oort cloud with an isotropic distribution in velocity space, the equivalent of a background gas at a temperature of a few millikelvin (Fig. 7). Second, we investigate the contribution to heating for the case of an Oort cloud with ''pendulum'' trajectories for all atoms in the cloud. The latter clearly is an upper limit to the heating rate due to the Oort cloud.

A. Isotropic gas model

We consider collisions of atoms in the Oort cloud with atoms in the sample at the center of the trap, assuming an isotropic distribution of the velocity of the atoms in the Oort cloud. The expression for the heating rate is then the same as for heating by primary collisions with a background gas, of course, with its composition and a much lower temperature T_{Oort} as the two most pronounced differences. First, the Oort cloud consists of the trapped species: the alkali-metal–alkali-metal long-range interaction is much stronger than the noble-gas-alkali-metal interaction, resulting in a much smaller value of $\mathcal{E}_{\text{ref}}$. Second, the mK temperature of the Oort cloud results in a scaling of the reference value $\mathcal{E}_{\text{ref}}$ to even lower values [Eq. (13)] as compared to the room-temperature value. The resulting value at $T_{\text{Oort}} = 2$ mK is $\mathcal{E}_{\text{ref,Oort}} = 125$ μK. For this reason primary collisions dominate the heating by collisions with atoms in the Oort cloud. The density $n_{\text{Oort}} \approx 10^6$ cm^{-3} corresponds to an equivalent background pressure of 3×10^{-11} Torr, not very different from the background gas itself at a trap loss lifetime of 100 s.

For Rb we can still apply—although marginally—the semiclassical expressions for the energy-transfer integral $\mathcal{I}_{QE}$ at an energy of a few mK (see the Appendix). The energy-transfer rate per atom is then given by [4]

$$\dot{U}_{\text{Oort}}/N = n_{\text{Oort}} v_{\text{Oort}} \mathcal{I}_{QE,\text{Oort}}. \quad (29)$$

Here, $v_{\text{Oort}} = (2k_B T_{\text{Oort}}/m)^{1/2}$ is the characteristic velocity of the atoms in the Oort cloud.

The calculation of $\mathcal{I}_{QE,\text{Oort}}$ has been done for the two different values $\mathcal{E}_{\text{eff}} = 200$ and 400 μK of the effective cutoff, i.e., the transition point between heating and trap-loss collisions. Because the cutoff is always much larger than the reference value, we can apply an approximate expression for the energy-transfer integral based on classical scattering [Eq. (10)]. In the Appendix we investigate the validity of this—rather crude—approximation, showing that the errors are not too large. Using the input as given in Table III, which applies to the case of Rb, we find an extra energy transfer rate in the range of 25–45 nK/s. Applying an rf shield, with a cutoff energy equal to $\mathcal{E}_{\text{rf}} = 48$ μK, as relevant for a comparison with the experimental results of Myatt [7], results in an extra energy-transfer rate equal to 7 nK/s.

Comparison to experimentally obtained heating rates shows that we cannot neglect this contribution of the Oort cloud to the energy-transfer rate to the centrally located cold sample. This extra contribution can perhaps explain why our model results in Sec. VII are always smaller than the experimental results of Myatt. In Table IV we compile the relevant data of Tables II and III for an easy comparison of the experimental and model results for the total heating rate in the

TABLE V. Calculated energy-transfer rates for secondary and primary collisions, in comparison with the experimental values for the heating rate in the ^{85}Rb trapping experiment at JILA. Due to the low value $\langle nl \rangle = 4 \times 10^{13}$ cm^{-3} of the column density, the contribution by primary collisions is larger than for secondary collisions.

	Background	$\mathcal{E}_{\text{eff}} = 200$ μK	$\mathcal{E}_{\text{eff}} = 400$ μK
Secondary collisions	He	1.1 nK/s	1.6 nK/s
Primary collisions	He	1.8 nK/s	7.0 nK/s
Experiment[a]		1–3 nK/s	

[a]Reference [18].

experiment of Myatt. We observe a rather good agreement on the absolute value.

An important observation that we cannot discard directly, however, is the fact that the extra contribution of the Oort cloud does *not* directly depend on the density or column density of the trap, as can be seen in Eq. (29). However, it is not unlikely that the density n_{Oort} of the Oort depends on the trap parameters such as the total population N or the trapping frequency. In turn, this would result in a dependency of the Oort contribution to the heating rate on the density and/or column density of the trap. A conclusive answer cannot be given: the experimental evidence on the Oort cloud is still too scarce.

B. Pendulum model

All atoms in the Oort cloud originate from a primary or secondary collision occurring in the sample at the center of the trap. When assuming an ideal harmonic trap, these atoms will acquire no additional macroscopic angular momentum. Their path in the trap volume will oscillate from one end of the trap to the other, each time traversing the sample at the center of the trap: a ''pendulum mode'' of atomic motion. This mode has been assumed as being effective for the rapid thermalization of the hot atoms with an energy below the cutoff energy $\mathcal{E}_{\text{eff}}$. This implies a very strong correlation of the velocity distribution and the spatial distribution of the atoms in the Oort cloud, with a strong collisional coupling to the sample in the center.

When we assume that this ''pendulum'' model applies to *all* atoms in the Oort cloud, we find extremely large values of the energy-transfer rate in the range of 100–400 μK/s. The magnitude of the calculated energy-transfer rate is typically a factor 1000 larger than experimental results. The major deficiency is the assumption that *all* atoms in the Oort cloud behave in a ''pendulum'' mode, crossing the sample in the center twice per oscillation period of the trapping potential. Clearly, this is not a realistic assumption, as already discussed in Sec. V B: the pendulum model is only realistic for the very-low energy atoms of the Oort cloud. However, this is precisely the regime where $E \lesssim \mathcal{E}_{\text{eff}}$ holds and the Oort cloud is depopulated in our newly proposed concept.

IX. COMPARISON TO ^{85}Rb EXPERIMENTS

Recently, great progress has been made in the trapping and cooling of the ^{85}Rb isotope. In 1999 these efforts have resulted in the observation of a condensate. However, both the density and the total number of trapped atoms are much smaller than in ^{87}Rb. Typical experimental heating rates are in the range of 1–3 nK/s. Applying a rf shield does not influence these rates. The heating rate is attributed to three-body collision loss rates. Above the transition temperature, characteristic numbers are $N = 10^6$, $\langle n \rangle = 5$ 10^{11} cm^{-3}, and $T = 50$ nK at confining frequencies of $17 \times 17 \times 7$ Hz^3 [18]. At these conditions, the typical dimensions in radial and axial direction are 21 and 40 μm, respectively, resulting in a column density of $\langle nl \rangle \approx 4$ 10^{13} m^{-2}. For this number we have used the radial dimension of the trap. The depth of the magnetic trap is on the order of a few mK. Typical trap-loss lifetimes are of the order of $\tau^p \approx 250$ s or more.

In Table V we present the energy-transfer rates for both secondary as well as primary collisions, again assuming an effective trap depth of $\mathcal{E}_{\text{eff}} = 200$ or 400 μK. Because the column density is rather low in this experiment, the energy-transfer rate for primary collisions is larger by a factor 2–3 than the contribution by secondary collisions. This occurs when the transition point $\mathcal{E}_X$ lies below the cutoff value $\mathcal{E}_{\text{eff}}$. We observe that the calculated heating rates are larger than the experimental values. Also, the calculated values would decrease when applying a rf shield, which is not observed experimentally.

A possible explanation can be found in the original assumption that three-body losses dominate the process of trap loss. The contribution of background collisions to the measured trap-loss lifetime $\tau^p = 250$ s is then much smaller, resulting in an effective lifetime for background collisions $(\tau^p)' \gg 250$ s. For example, $(\tau^p)' = 1000$ s results in a decrease by a factor 4 in the calculated heating rates, showing a better agreement of calculation and experiment. It is rather hard to find another idea to obtain a smaller value of the primary-collision heating rate, due to its very direct relationship to the primary-collision loss rate. This discussion confirms the assumption that the experimentally observed heating rate should be partially attributed to other processes than primary and secondary collisions driven by the background gas.

X. CONCLUDING REMARKS

All trapping experiments that lead to Bose-Einstein condensation are in the collisionally opaque regime when they

are close to the transition temperature. The simple model of density-independent heating by primary collisions with the background gas is then no longer valid. In this case, secondary collisions inside the trap are the main cause of heating, with only a small contribution from primary collisions with the background gas and tertiary collisions with atoms in the Oort cloud. Lowering the trap depth has no influence on the secondary heating rate, because the cutoff between heating and loss collisions is determined by an escape into the Oort cloud rather than the escape from the trap.

A very efficient method to decrease the heating rate in a trap is to apply a rf shield, as shown experimentally. The model in this paper supports this conclusion both quantitatively as well as qualitatively. Another efficient way to decrease the secondary heating rate while keeping the density in the trap high is to opt for a trap geometry with a large aspect ratio, i.e., a trap with a strong radial confinement and a very relaxed axial confinement. In this case the radial dimension will be the relevant length parameter that determines the column density in Eq. (21). This conclusion is the same as for a trap of metastable neon atoms, where secondary collisions of the hot products of ionizing collisions in the trap are the major source of heating [15].

Finally, the non-negligible contribution of collisions with atoms in the Oort cloud to the heating rate shows us that it is important to obtain quantitative data on its population. Only then can we give a final answer to questions such as the dependency of the population of the Oort cloud on the trap parameters. Also, more insight is necessary with respect to the dynamics of the formation of the Oort cloud. Is the Oort cloud a remnant of the population of the magneto-optical trap which has ''survived'' the process of evaporative cooling? These questions are the motivation for future research on the Oort cloud.

APPENDIX: ELASTIC CROSS SECTIONS

1. Semiclassical approach

Within the framework of a semiclassical approach to elastic scattering, the small-angle differential cross section $\sigma(\theta)$ scales with the diffraction angle $\theta_0 = (4\pi/k^2 Q)^{1/2}$, with k the wave number. For an inverse power law potential $V(R) = C_6/R^6$ the total cross section Q, the differential cross sec-

TABLE VI. Elastic total cross section $Q_{T\to 0}$ and differential cross section $\sigma_{T\to 0}(0)$ for Rb in the limit of s-wave scattering, together with the scattering length a. For comparison we also give the numerical result when evaluating the semiclassical expressions for Q, $\sigma(0)$, and θ_0 at a center-of-mass energy $E_{cm}=E/2 = 39$ μK at the transition point to pure s-wave scattering, far outside the range of validity. We observe that the absolute values are in fair agreement. Also, the isotropic differential cross section $\sigma_{T\to 0}(0)$ for s-wave scattering is fairly well characterized over a large angular range by the semiclassical expression with a characteristic angle $\theta_0 = 1.8$ rad.

Regime	Parameter	Value
s wave	a	$100a_0$
	$Q_{T\to 0}$	7×10^4 Å^2
	$\sigma_{T\to 0}(0)$	5.6×10^3 Å^2/sr
	$\sigma_{T\to 0}(\theta)$	isotropic
Semiclassical	Q	5×10^4 Å^2
	$\sigma(0)$	2.9×10^3 Å^2/sr
	θ_0	1.83 rad

tion $\sigma(0)$ for scattering in the forward direction and the diffraction angle θ_0 are related according to

$$Q = 8.08(C_s/\hbar v)^{2/(s-1)},$$

$$\sigma(0) = k^2 Q^2/[16\pi^2 \cos^2(\pi/5)],$$

$$\theta_0 = (4\pi/k^2 Q)^{1/2}, \tag{A1}$$

$$2\pi\theta_0^2 \sigma(0)/Q = [2\cos^2(\pi/5)]^{-1} = 0.764.$$

Throughout this paper we use semiclassical expressions for both the total cross section as well as the differential cross section. For the primary collisions at $E_b/k_B = 300$ K this is a highly accurate description of fully quantum-mechanical calculations. For the secondary collisions, at energies in the few millikelvin to tens of K range, we have to establish the range of collision energies where this approximation still applies within reasonable accuracy.

2. Quantum mechanical calculations

In Fig. 8 we show the fully quantum mechanical total cross section for Rb-Rb collisions [16], as a function of the center-of-mass energy E_{cm}. The partial waves $l=0$, 2, 4, and 6 have been taken into account in these calculations. For $E_{cm} \lesssim 39$ μK we indeed observe that the total cross section is nearly constant, indicative for s-wave scattering. For pure s-wave scattering the elastic cross section is fully determined by the scattering length a, as given by

$$Q_{T\to 0} = 8\pi a^2, \tag{A2}$$

$$\sigma_{T\to 0}(\theta) = Q_{T\to 0}/4\pi. \tag{A3}$$

The differential cross section is isotropic in this limit, as expected for an incoming s wave. For comparison, we have

also plotted the semiclassical expression for Q, as given in Eq. (A1). For a center-of-mass energy $E_{cm}=E/2\gtrsim 4$ mK the semiclassical result agrees with the quantum-mechanical total cross section within a factor of 2.

3. Range of validity of semiclassical approach

The height of the rotational barrier for p-wave scattering defines the characteristic center-of-mass energy $E_{p\text{-}wave}$ which defines the onset of multiple partial-wave scattering. The semiclassical expressions for the total and differential cross section provide a sufficiently accurate description of fully quantum-mechanical calculations when 5–10 partial waves contribute to the Rayleigh sum for the scattering amplitude. This condition is thus satisfied at a center-of-mass energy that is larger by a factor of 64–256 (for bosons only even partial waves contribute), because the deBroglie wavelength scales as $E_{cm}^{-1/2}$. For Rb, with $E_{p\text{-}wave}=39$ μK, this implies a lower limit of $E=2E_{cm}=5$ to 20 mK for the range of validity of our semiclassical approach.

Surprisingly, the absolute value and the general character of the s-wave cross section and the (incorrectly applied) semiclassical expressions at a laboratory energy equal to the onset of the s-wave scattering regime are not very disparate for Rb, as can be seen in Table VI. The absolute values of Q and $\sigma(0)$ are equal to $Q_{T\to 0}$ and $\sigma_{T\to 0}(0)$ within 30% and 40%, respectively. The characteristic angle is equal to $\theta_0 = 1.83$, indicating a rather isotropic differential cross section over a large angular range. This is in fair agreement with the isotropic differential cross section for s-wave scattering. Of course, features like the $l=2$ resonance in the cross section are not incorporated in the semiclassical formulas.

For the calculation of the energy-transfer rate by secondary collisions, the lower limit of the energy E_β is equal to the effective trap depth $\mathcal{E}_{\text{eff}}$, which is on the order of 400 μK. However, for He-Rb primary collisions with a reference value $\mathcal{E}_{\text{ref},b}^p=17.5$ mK, the majority of the collisions result in a transferred energy $E_\beta>8$ mK. The fraction of the collisions with a smaller transferred energy is equal to $\Delta Q_b^p(8\ \text{mK})/Q_b^p=0.38(8\ \text{mK}/\mathcal{E}_{\text{ref},b}^p)=0.17$. The range of validity of the semiclassical expressions is thus fairly well matched to the range of application in the energy-transfer integral $\mathcal{I}_{QE,\beta}$. We conclude that the calculated energy-transfer rates by secondary collisions are reliable for all practical applications, with an estimated error on the order of 25% or less.

[1] M. Anderson *et al.*, Science **269**, 198 (1995).

[2] K. Davis *et al.*, Phys. Rev. Lett. **75**, 3969 (1995).

[3] C. Bradley, C. Sackett, J. Tollett, and R. Hulet, Phys. Rev. Lett. **75**, 1687 (1995).

[4] H. Beijerinck, Phys. Rev. A **61**, 033606 (2000).

[5] V. Vuletic, C. Chin, J. Kerman, and S. Chu, Phys. Rev. Lett. **81**, 5768 (1998).

[6] S. Bali *et al.*, Phys. Rev. A **60**, R29 (1999).

[7] C. Myatt, Ph.D. thesis, University of Colorado, Boulder, 1997.

[8] E. Cornell, J. Ensher, and C. Wieman, in *Bose-Einstein Condensation in Atomic Gases*, *Proceedings of the International School of Physics, Enrico Fermi*, edited by M. Inguscio, S. Stringari, and C. Wieman (IOS Press, Amsterdam, 1999), p. 15, course CXL.

[9] H. Pauly, *Physical Chemistry*, edited by W. Jost (Academic Press, New York, 1975), Vol. 6B, p. 553.

[10] D. Beck, in *Molecular Beams and Reaction Kinetics*, edited by C. Schlier (Academic Press, New York, 1970), p. 15.

[11] H. Beijerinck, P. van der Kam, W. Thijssen, and N. Verster, Chem. Phys. **45**, 225 (1980).

[12] K. Ford and J. Wheeler, Ann. Phys. (N.Y.) **7**, 259 (1959).

[13] K. Ford and J. Wheeler, Ann. Phys. (N.Y.) **7**, 287 (1959).

[14] J. Oort, Bull. Astron. Inst. Neth. **11**, 91 (1950).

[15] H. Beijerinck *et al.*, Phys. Rev. A **61**, 023607 (2000).

[16] S. Kokkelmans and B. Verhaar (private communication).

[17] S. Kokkelemnas, B. Verhaar, K. Gibble, and D. Heinzen, Phys. Rev. A **56**, R4389 (1997).

[18] J. Roberts and C. Wieman (private communication).

[19] A. Derevianko, W. Johnson, M. Safronova, and J. Babb, Phys. Rev. Lett. **82**, 3589 (1999).

[20] T. Proctor and W. Stwalley, J. Chem. Phys. **66**, 2063 (1977).